Stem Cell Reports
Article
ISSCR
OPEN ACCESS

Niclosamide induces *miR-148a* to inhibit PXR and sensitize colon cancer stem cells to chemotherapy

Lucile Bansard,[1,6] Océane Bouvet,[1,6] Elisa Moutin,[1] Gaétan Le Gall,[1] Alessandro Giammona,[1] Elodie Pothin,[1] Marion Bacou,[1] Cédric Hassen-Khodja,[2] Benoit Bordignon,[2] Jean François Bourgaux,[3] Michel Prudhomme,[3] Frédéric Hollande,[4,5] Julie Pannequin,[1] Jean Marc Pascussi,[1,7,*] and Chris Planque[1,7,*]

[1]IGF, Université de Montpellier, CNRS, INSERM, Montpellier, France
[2]Montpellier Ressources Imagerie, Biocampus, Université de Montpellier, CNRS, INSERM, Montpellier, France
[3]CHU Carémeau, Nîmes, France
[4]Department of Clinical Pathology, The University of Melbourne, Victorian Comprehensive Cancer Centre, Melbourne, VIC 3000, Australia
[5]University of Melbourne Centre for Cancer Research, Melbourne, VIC 3000, Australia
[6]These authors contributed equally
[7]These authors contributed equally
*Correspondence: jean-marc.pascussi@inserm.fr (J.M.P.), chris.planque@igf.cnrs.fr (C.P.)
https://doi.org/10.1016/j.stemcr.2022.02.005

SUMMARY

Tumor recurrence is often attributed to cancer stem cells (CSCs). We previously demonstrated that down-regulation of Pregnane X Receptor (PXR) decreases the chemoresistance of CSCs and prevents colorectal cancer recurrence. Currently, no PXR inhibitor is usable in clinic. Here, we identify *miR-148a* as a targetable element upstream of PXR signaling in CSCs, which when over-expressed decreases PXR expression and impairs tumor relapse after chemotherapy in mouse tumor xenografts. We then develop a fluorescent reporter screen for *miR-148a* activators and identify the anti-helminthic drug niclosamide as an inducer of *miR-148a* expression. Consequently, niclosamide decreased PXR expression and CSC numbers in colorectal cancer patient-derived cell lines and synergized with chemotherapeutic agents to prevent CSC chemoresistance and tumor recurrence *in vivo*. Our study suggests that endogenous miRNA inducers is a viable strategy to down-regulate PXR and illuminates niclosamide as a neoadjuvant repurposing strategy to prevent tumor relapse in colon cancer.

INTRODUCTION

Colorectal cancer (CRC) is the third most commonly diagnosed cancer worldwide, responsible for 10% of cancer incidence and mortality despite diagnostic and therapeutic advances (Siegel et al., 2017). The principal CRC chemotherapeutic regimens are 5-fluorouracil, irinotecan, and/or oxaliplatin. The combination of these chemotherapeutic regimens with targeted therapies has further improved survival. However, treatment fails in 90% of cases once the disease becomes metastatic. Therapeutic resistance and tumor recurrence are thought to be caused by a subpopulation of tumor cells, termed cancer stem cells (CSCs) (Adorno-Cruz et al., 2015; Prud'homme, 2012). Unlike most cells in a tumor, CSCs can self-renew. CSCs strongly metabolize cytotoxic compounds, leading to their enrichment following treatment (Todaro et al., 2007), and their self-renewal abilities allow the subsequent initiation of tumor relapse (Dylla et al., 2008; Planque et al., 2016). Therefore, as well as targeting highly proliferative cancer cells, an effective CRC therapy must also efficiently eliminate colon CSCs.

We previously reported that CSCs drive post-treatment recurrence in colon cancer by overexpressing Pregnane X Receptor (PXR) protein (NR1I2) (Planque et al., 2016). PXR is a transcription factor that belongs to the nuclear hormone receptor superfamily (Lehmann et al., 1998). We demonstrated that PXR is needed for CSC self-renewal and the expression of key CSC-related chemoresistance genes (such as *CYP3A4*, *ALDH1A1*, and *ABCG2*). Furthermore, siRNA-based *PXR* knockdown increases chemosensitivity of CSCs, delaying post-chemotherapy tumor relapse (Planque et al., 2016). Accordingly, we (Planque et al., 2016) and others (Dong et al., 2017) have linked high levels of PXR expression with poor recurrence-free survival in colon cancer patients after chemotherapy. Taken together, these data point to PXR as a target to improve the efficiency of chemotherapy and counteract the selection and emergence of chemo-resistant CSCs and avoid post-treatment tumor recurrence.

The race is now on to translate these recent findings into a clinical therapeutic. However, although nuclear receptors usually respond to a specific set of high-affinity ligands, PXR is activated by a broad spectrum of low-affinity xenobiotics, and crystallographic studies revealed a ligand binding domain (LBD) with a large and conformable binding pocket that renders it extremely difficult to identify PXR antagonists using *in silico* or conventional medicinal chemistry approaches. Accordingly, only a few antagonists were described to date—SPA-70 (Lin et al., 2017), L-sulforaphane (Zhou et al., 2007), or ketoconazole (Huang et al., 2007)—but their efficacy (Poulton et al., 2013) and safety remain inappropriate for clinical use (Fuchs et al., 2013). One of the means to down-regulate a protein of interest is the

use of microRNA (miRNA) (Huang, 2017). miRNAs are small, noncoding RNAs that are approximately 20–25 nt in length. They regulate the expression of multiple target genes through sequence-specific hybridization to the 3′ untranslated region (UTR) of messenger RNAs, blocking their translation or causing their degradation. Indeed, *in vitro* experiments have previously identified that *miR-148a-3P* (*miR-148a*) directly participates in the post-transcriptional regulation of *PXR* in human hepatocytes (Rao et al., 2017; Takagi et al., 2008) and in oropharyngeal cancer cells (Reuter et al., 2019). In addition, it has been reported that *miR-148a* expression is lower in breast CSCs compared with non-CSCs (Boo et al., 2017). Moreover, the down-regulated expression of this miRNA is detected in various cancers, including gastric and colorectal, where, in contrast with *PXR* (Dong et al., 2017; Planque et al., 2016), high miR-148a expression is a good prognostic indicator in both early-stage (Igder et al., 2019) and treated metastatic CRC (Shivapurkar et al., 2014; Takahashi et al., 2012; Tsai et al., 2013).

Here, we demonstrate that *miR-148a* overexpression suppressed the expression of PXR and CSC chemoresistance both *in vitro* and *in vivo*. Because *in vivo* synthetic miRNA delivery remains an unsolved obstacle (Pecot et al., 2011), we developed a high-content cell-based fluorescent reporter system to identify niclosamide as a potent inhibitor of PXR expression via the induction of *miR-148a*. This strategy may be of therapeutic value in colon cancer and provide the basis for repurposing this anthelmintic drug as an adjuvant strategy to reduce CSC chemoresistance.

RESULTS

miR-148a level is inversely correlated with PXR expression in CRC cells and is down-regulated in CSCs

miR-148a-3p (*miR-148a*) has been reported to post-transcriptionally regulate *PXR* expression (Rao et al., 2017; Reuter et al., 2019; Takagi et al., 2008). This miRNA is positively correlated with the clinical outcome of treated-metastatic CRC patients, whereas the opposite is true for *PXR* (Dong et al., 2017; Planque et al., 2016; Takahashi et al., 2012; Tsai et al., 2013). We thus suspected that this miRNA would anti-correlate with the agency of *PXR* in CRC cells. Using RT-qPCR, we observed that *PXR* and *miR-148a* mRNAs were negatively correlated ($r = -0.697$, $p = 0.0038$) in a panel of CRC cell lines (T84, SW620, HT29, LS174T, and HCT116) and patient-derived colon cancer cell lines established in our laboratory: from primary (CPP1, CPP6, CPP14, CPP24, CPP25, CPP35) and metastatic (CPP19, CPP30, CPP36) tumors or blood (circulating cancer cells, CTC44, Grillet et al., 2017) (Figure 1A). We also observed that the expression of PXR downstream target genes, such as *ALDH1A1* (Planque et al., 2016) (Figure 1B), was inversely correlated with *miR-148a* expression ($r = -0.677$, $p = 0.0055$).

Because it has been reported that *miR-148a* expression is lower in spheroid-enriched breast CSCs compared with non-CSCs (Boo et al., 2017), we hypothesized that such a mechanism may contribute to the preferential expression of PXR in colon CSCs. We quantified *miR-148a* expression in CSCs that we had enriched from CRC cells by several approaches: isolation of cells with high ALDH (aldehyde dehydrogenase) enzymatic activity (considered as a robust CSC marker) (Ginestier et al., 2007), non-CSC depletion or reprogramming via chemotherapy treatment (Firi = 5-FU [fluorouracil] + SN-38) (Kreso et al., 2013; Todaro et al., 2007), and maintenance as colonospheres (Spheres) (Kanwar et al., 2010). We observed that expression of *miR-148a* was significantly lower in both CPP1 patient-derived CRC cells or in the metastatic CRC cell line (SW620) under conditions that enrich CSCs, i.e., ALDH-positive cells, Spheres, or after Firi treatment (Figures 1C and 1D), compared with non-CSCs, i.e., untreated (2D-UT), non-sorted (NS), or ALDH-negative cells. Moreover, as shown in Figures 1E and 1F, we observed a negative correlation between the expression of *PXR* mRNA or protein and *miR-148a* mRNAs in CPP1 cells according to their status: higher expression of *PXR* in CSCs ($ALDH^{pos}$ and Spheres) compared with non-CSC ($ALDH^{neg}$ and 2D-UT) conditions, and the opposite for miR-148a. We also observed that the expressions of PXR downstream target genes *ALDH1A1* and *ABCG2* were inversely correlated with *miR-148a* expression (Figures S1A and S1B). These results confirm that *miR-148a* level is negatively correlated with PXR expression in colorectal CSCs, suggesting that low *miR-148a-3p* expression may enable the preferential expression of PXR in these cells.

Overexpression of miR-148a represses the PXR expression and PXR signaling pathway

We then confirmed the causal relationship between *miR-148a* and PXR expression and/or activity. CRC cells were transfected with synthetic miRNA Mimic *miR-148a-3p* (*miR-148a*) or the mirVana microRNA Mimic Negative Control #1 (miCTRL). Two days after transfection, we observed a decrease of *PXR* and PXR target genes, such as *ALDH1A1*, *FGF19* (Wang et al., 2011), or *ABCG2* mRNAs in *miR-148a*-transfected cells compared with control cells (Figures 2A and S2A). *DNMT1*, a well-described *miR-148a* target gene (Yan et al., 2014), was used as positive control of *miR-148a* transfection. To monitor the effect of *miR-148a* on PXR protein expression and transcriptional activity, we then performed western blot analyses and gene reporter assays. First, we observed a decrease of PXR protein level in HT29 cells transfected with the

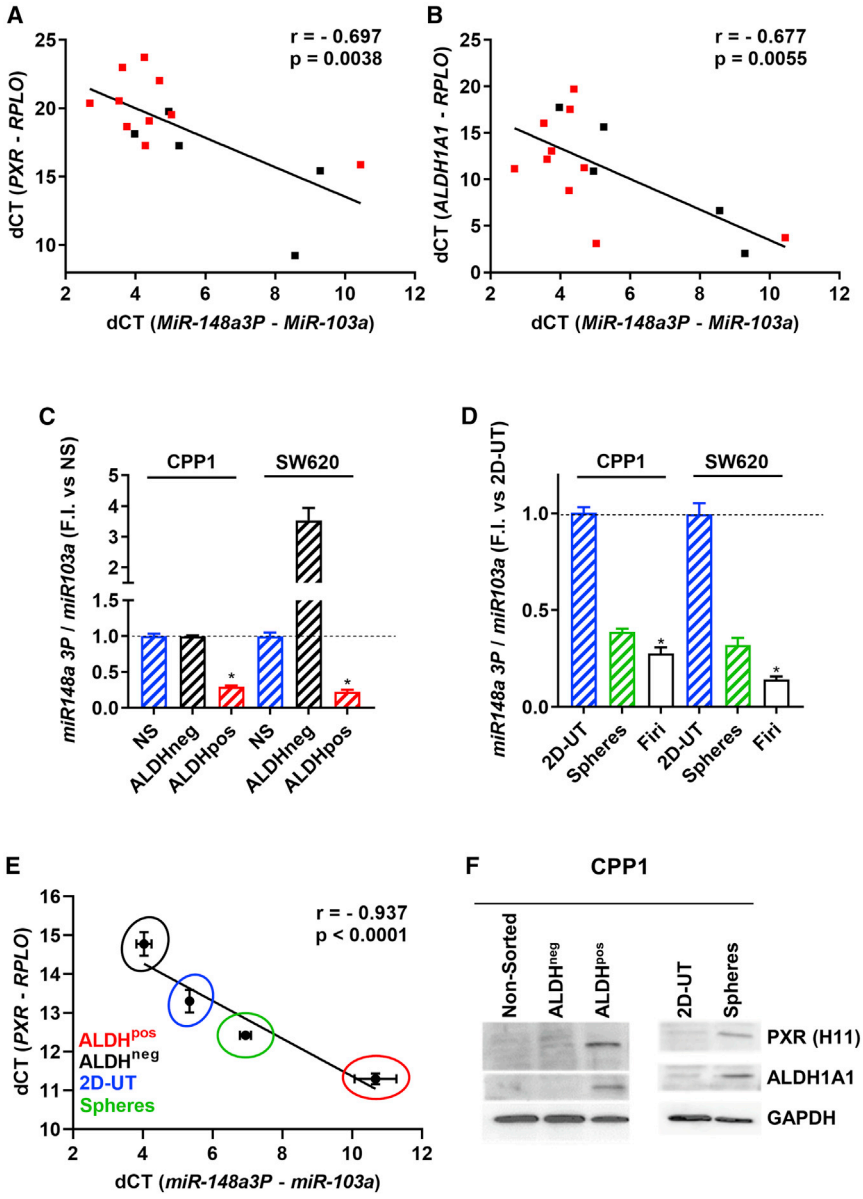

Figure 1. miR-148a is inversely correlated with PXR in CRC and is down-regulated in CSCs

(A and B) Inverse correlation between *PXR* or PXR target gene (*ALDH1A1*) (A) and *miR-148a* (B) expression in CRC cell lines purchased from ATCC (T84, SW620, HT29, LS174T, and HCT116, black squares) and patient-derived CRC cells established in the laboratory (primary [CPP1, CPP6, CPP14, CPP24, CPP25, CPP35]; metastatic [CPP19, CPP30, CPP36] or circulating cancer cells [CTC44], red squares) by RT-qPCR analyses (n = 2). The expression of *PXR* was normalized to RPLO ((60S acidic ribosomal protein P0)), while expression of *miR-148a-3p* was normalized to *miR-103a-3p*.

(C and D) *miR-148a-3p* expression in patient-derived CPP1 and SW620 colon cancer cells after cell sorting based on Aldefluor activity (ALDH-negative and -positive population) (C), or after 72 h of chemotherapy treatment (FIRI = 5μM 5-FU + 50 nM SN38) or maintained as colonospheres (Spheres) (D). Data are expressed as mean ± SEM (n = 3). F.I., fold induction compared with non-sorted cells (NS) or untreated cells grown under adherent conditions (2D-UT).

(E and F) Negative correlation between *PXR* and miR-148a expression (data are expressed as mean ± SEM, n = 3) (E), and western blot analysis of PXR and ALDH1A1 protein expression levels (F) in CSCs (ALDH-positive cells [$ALDH^{pos}$] and Spheres) and non-CSCs (NS cells, cells grown under adherent conditions [2D-UT] and ALDH-negative cells [$ALDH^{neg}$]) from patient-derived CPP1 cells. *p < 0.05.

miR-148a-3p Mimic (*miR-148a*) compared with the miCTRL negative control (Figure 2B). In addition, we observed a significant decrease of PXR transcriptional activity (*CYP3A4* promoter-driven luciferase, Drocourt et al., 2002) in *miR-148a* co-transfected HT29 or CPP1 cells compared with cells transfected with the miCTRL (Figure 2C). In accordance, the proportion of cells with high ALDH activity was also decreased in CRC cells transfected with the *miR-148a-3p* mimic compared with the miCTRL (Figures 2D and S2B) as a result of lower *ALDH1A1* mRNA expression. Similar results were observed in HT29 cells infected with a lentivirus (pMIRNA) allowing the stable expression of miRNA and the copGFP (green fluorescent protein from the copepod Pontellina plumata) used for monitoring transfection efficiency and sorting. After purification and expansion of green fluorescent protein (GFP)-positive cells, we observed a down-regulation of *PXR* and PXR target gene mRNA expression (Figure S2C) and the proportion of cells with high ALDH activity (Figure S2D) in cells injected with a lentivirus encoding *miR-148a* (miR-148a/copGFP) compared with control cells (i.e., infected with the control copGFP lentivirus [CTRL/copGFP]).

Overexpression of miR-148a represses the CSC phenotype

To test the functional significance of *miR-148a*-mediated PXR down-regulation in CSCs, we transfected CRC cell lines with synthetic miRNA mimics. Overexpression of

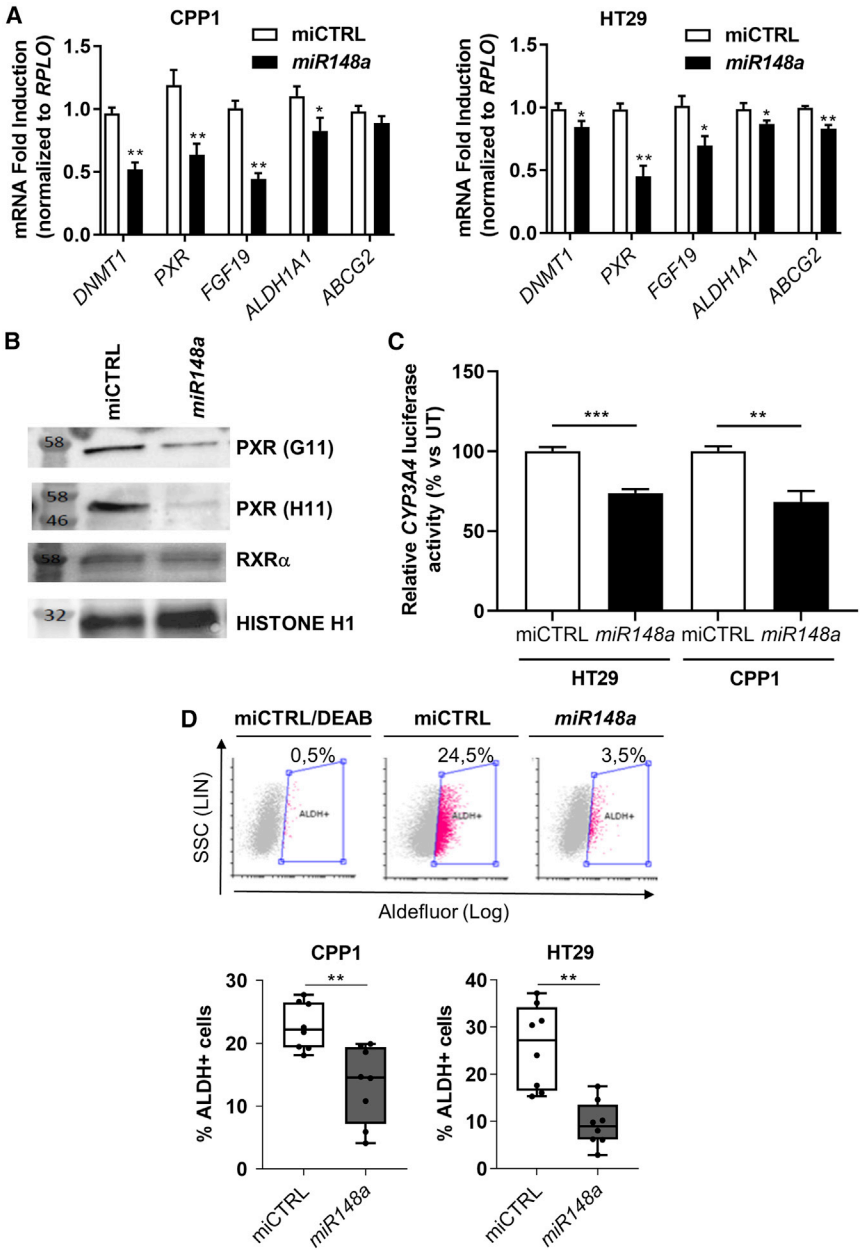

Figure 2. Overexpression of miR-148a represses PXR signaling

(A) RT-qPCR analyses of *DNMT1*, *PXR*, and PXR target gene mRNA expression in CPP1 (left panel) and HT29 (right panel) colon cancer cells transfected with *miR-148a-3p* (*miR-148a*) or mirVana microRNA Mimic Negative Control #1 (miCTRL) mimics. Data are expressed as mean ± SEM (n = 5). Fold induction compared with cells transfected with negative control mimic.

(B) Western blot analysis of PXR (with two anti-PXR antibodies G11 and H11), RXRα, and Histone H1 expression in HT29 cells transfected with *miR-148a-3p* or miCTRL mimics.

(C) PXR transcriptional activity was determined in HT29 and CPP1 cells transfected with *miR-148a-3p* or miCTRL mimics, 24 h after transfection with a PXR-responsive (NR1)3TKluc (*PXR*E TKLuc) luciferase reporter plasmid. Data are expressed as mean ± SEM (n = 3) normalized to non-transfected cells (UT).

(D) Quantification of ALDH activity using the Aldefluor assay in CPP1 and HT29 colon cancer cells transfected with *miR-148a-3p* or miCTRL mimics. Percentage of Aldefluor-positive cells ($ALDH^+$) is indicated in inset boxes for a representative experiment in CPP1 cells (upper panel). Data are expressed as mean ± SEM (n = 8). *p < 0.05, **p < 0.005, ***p < 0.001.

miR-148a significantly decreased CD44v6-positive cells (Figure 3A) and *CD44v6* mRNA expression (Figure S3A) compared with cells transfected with the microRNA Mimic Negative Control (miCTRL). CD44v6 has been reported as a membrane marker of colorectal CSC (Ma et al., 2019; Todaro et al., 2014). Next, we tested the impact of the miRNA on the ability of colon cancer cells to form tumorspheres (Kanwar et al., 2010). As shown in Figures 3B and S3B, a reduced number of spheres was formed in CRC cells transfected with *miR-148a* mimic compared with cells transfected with the negative miCTRL. We noted that this inhibitory effect of *miR-148a* was not restricted to the primary spheres alone but also in the following generations (Figures S3C and S3D), suggesting that *miRNA-148a* reduces CSC self-renewal ability. Moreover, restoration of PXR expression via the use of a *PXR* cDNA construct devoid of the 3′UTR miR-148a-targeting sequence (Takagi et al., 2008) significantly reversed the *miR-148a* inhibitory effects on ALDH-positive cells (Figure 3C), sphere-forming ability (Figure 3D), and PXR target gene expression (Figure 3E) initially observed in HT29 *miR-148a*/copGFP cells. Indeed, these rescue experiments are evidence that *miR-148a*-insensitive PXR expression is sufficient to reverse

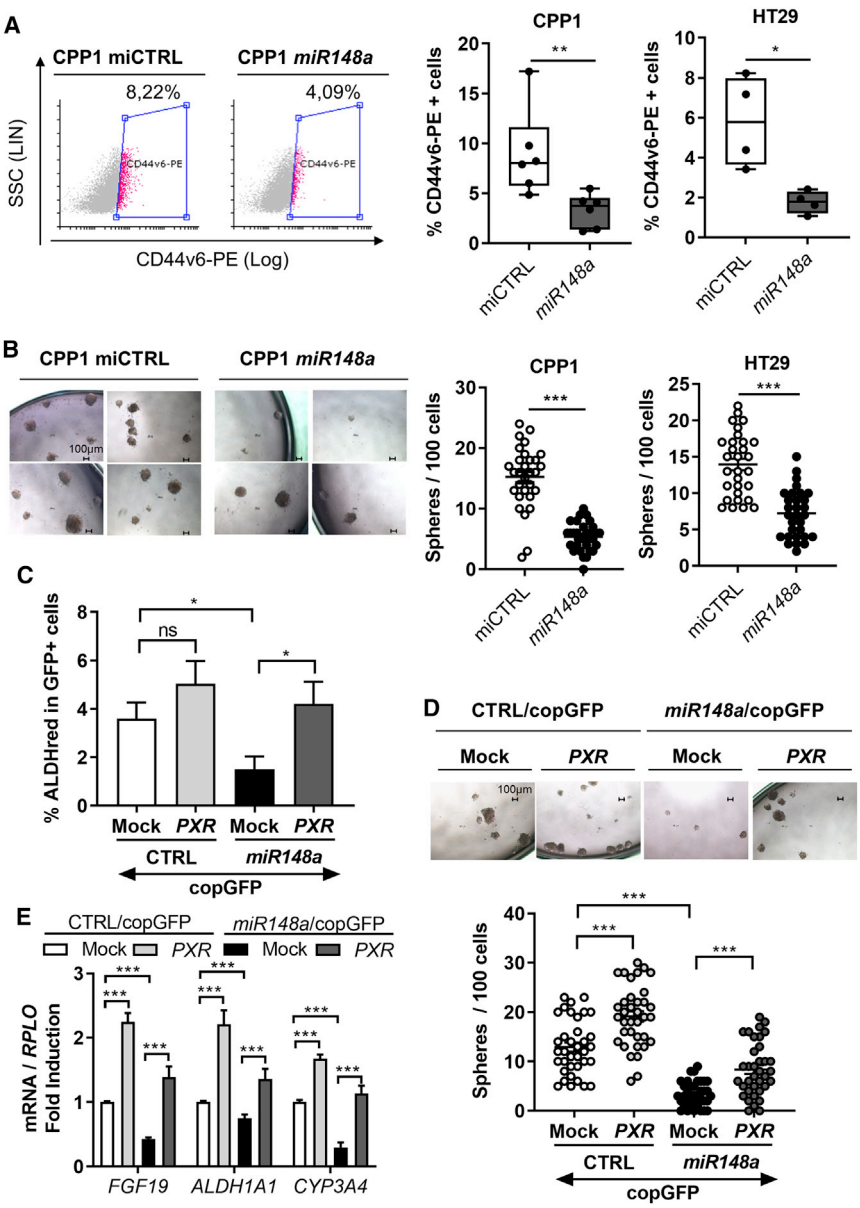

Figure 3. Overexpression of miR-148a represses the CSC phenotype *in vitro*

(A) Quantification of the CD44v6-PE-positive population in CPP1 (n = 6) and HT29 (n = 4) cells transfected with *miR-148a-3p* (*miR-148a*) or mirVana microRNA Mimic Negative Control #1 (miCTRL) mimics. Percentage of CPP1 CD44v6-PE-positive cells is indicated in inset boxes for a representative experiment (left panel).

(B) Representative pictures of tumorspheres (left panels) and percentage (right panels) of sphere-forming cells of patient-derived CPP1 and HT29 colon cancer cells transfected with *miR-148a-3p* or miCTRL mimics. Individual replicate values (n = 10 per experiment) are plotted, as well as the mean ± SEM (n = 3).

(C and D) Percentage of ALDH-positive cells (% of ALDHred, data are expressed as mean ± SEM, n = 6) (C) and representative pictures of tumorspheres (upper panels) and percentage (lower panel; data are expressed as mean ± SEM, n = 3 with 12 individual replicate values per experiment) (D) of sphere-forming cells in HT29 cells stably overexpressing *miR-148a* (*miR-148a*/copGFP) or empty sequence (CTRL/copGFP) transfected either with a miR-148a-insensitive *PXR* coding sequence (*PXR*) or the pcDNA3 empty vector (Mock).

(E) RT-qPCR analyses of PXR target gene (*FGF19*, *ALDH1A1*, *CYP3A4*) mRNA expression in HT29 cells stably overexpressing *miR-148a*/copGFP or CTRL/copGFP transfected either with a *miR-148a*-insensitive *PXR* coding sequence (*PXR*) or the pcDNA3 empty vector (Mock). Data are expressed as mean ± SEM (n = 3). *p < 0.05, **p < 0.005, ***p < 0.001.

miR-148a-mediated inhibition of CSC markers (*ALDH1A1*, *CYP3A4*) and self-renewal, supporting the hypothesis that PXR down-regulation is involved in miR-148a effects.

Overexpression of miR-148a impairs CSC chemoresistance and delays post-treatment recurrence in mouse xenograft models

Because PXR drives the expression of a large network of genes instrumental for CSC chemoresistance (including *ALDH1A1*, *ABCG2*, and *CYP3A4*; Planque et al., 2016), we assessed the impact of *miR-148a* overexpression on the survival of ALDH-positive patient-derived CRC cells treated *in vitro* with a cocktail of chemotherapy drugs for CRC (Firi = 5-FU + SN38). As shown in Figure 4A, transfection of ALDH-positive sorted cells with the *miR-148a* mimic significantly decreased their survival after 72 h of treatment with Firi (4-fold decrease of EC_{50} [half maximal effective concentration], $p < 0.05$), compared with cells transfected with a control mimic. In addition, as shown in Figure 4B, while the proportion of ALDH-positive cells was significantly increased after chemotherapy treatment in cells transfected with a control mimic, this enrichment was severely impaired in *miR-148a*-transfected cells, suggesting that *miR-148a* expression sensitizes CSCs to chemotherapy. To confirm these results *in vivo*, we generated tumor xenografts by subcutaneously injecting

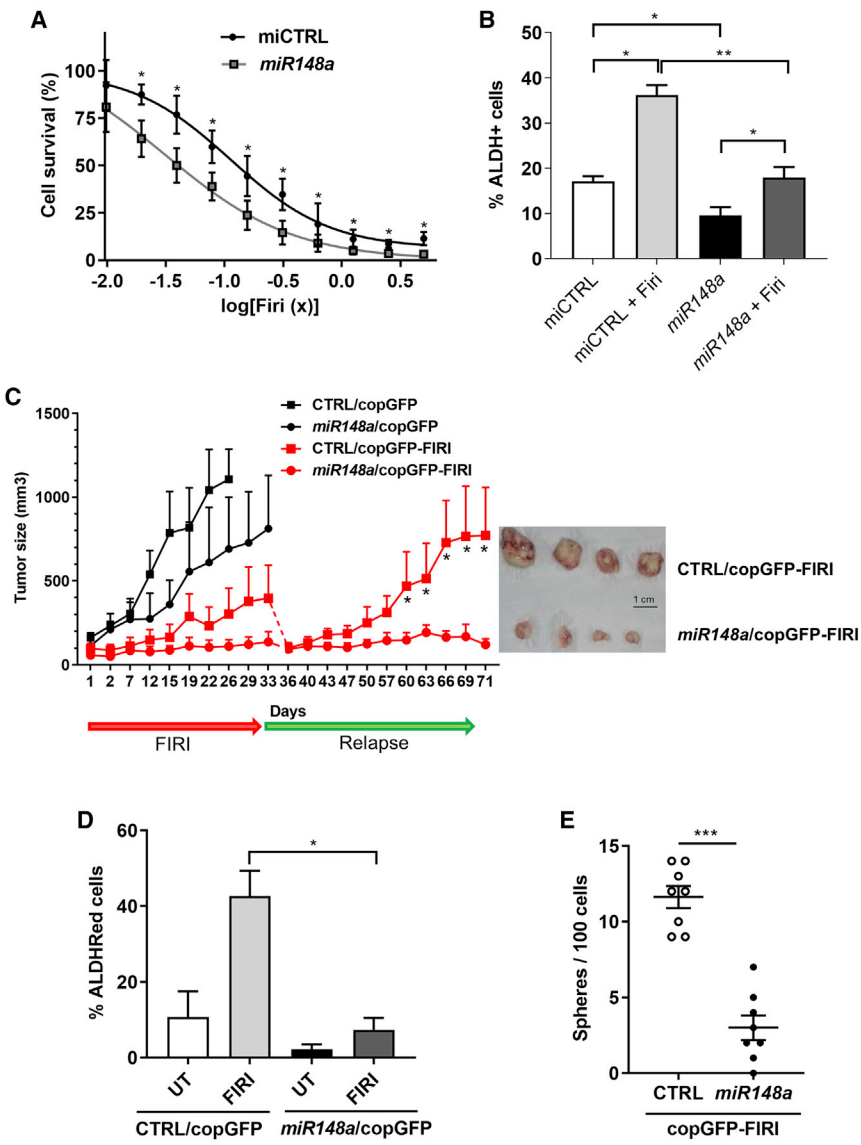

Figure 4. Overexpression of miR-148a impairs CSC chemoresistance and delays post-treatment recurrence

(A) Percentage of surviving CSCs (Aldefluor-positive cells) 48 h after exposure to the indicated concentrations of FIRI (1X = 50 μM 5-FU + 500 nM SN38) *in vitro*. Sorted CPP1 Aldefluor-positive cells were first transfected with 50 nM *miR-148a-3p* (*miR-148a*) or mirVana microRNA Mimic Negative Control #1 (miCTRL) mimics, 24 h prior to FIRI treatment. Data are expressed as mean ± SEM (n = 3).

(B) Percentage of Aldefluor-positive cells (% of ALDH + cells) in CPP1 cells transfected with miR-148a or miCTRL mimics and then exposed for 72 h to chemotherapy (Firi = 5 μM 5-FU + 50 nM SN38). Data are expressed as mean ± SEM (n = 5).

(C) Left panel: tumor volume over time after subcutaneous injection of HT29 cells stably overexpressing *miR-148a* (*miR-148a*/copGFP, n = 18 mice) or not (CTRL/copGFP, n = 18 mice). For each group, mice were randomized once tumors reached a volume of 100 mm^3: 6 mice were treated twice weekly with vehicle (black plots), 12 others with FIRI (50 mg/kg 5-FU and 25 mg/kg irinotecan, red plots). At day 33, six mice per group were sacrificed, and the remaining ones from the FIRI-treated groups were kept without treatment to further monitor tumor growth. Data are expressed as mean ± SEM. Right panel: pictures of xenograft tumors collected at day 71.

(D) Percentage of HT29 ALDHRed-positive cells recovered from resected tumors at day 33. Data are expressed as mean ± SEM (n = 4).

(E) Percentage of sphere-forming cells of live (7AAD-negative) HT29 cells (GFP^+) isolated from pooled tumor xenografts of FIRI-treated mice (CTRL/copGFP or *miR-148a*/CopGFP) at day 33 (mean ± SEM, n = 8). *p < 0.05, **p < 0.005, ***p < 0.001.

sphere-derived HT29-*miR-148a*/copGFP or control HT29-CTRL/copGFP cells into nude mice (n = 18 mice/group). Once tumors reached a volume of 100 mm^3, mice were randomized and received either vehicle (PBS, n = 6 mice/group) or FIRI cocktail (50 mg/kg 5-FU and 25 mg/kg irinotecan, n = 12 mice/group) twice a week for 4 weeks from day 1 to 29 (Figure 4C). First, we observed a better chemotherapy treatment response in miR-148a/copGFP xenografts compared with the control group. Four days after halting treatment (day 33), six mice from the PBS- and FIRI-treated groups were sacrificed for subsequent analysis, while tumor growth was monitored in the remaining FIRI-treated mice. As shown in Figure 4C, tumor recurred rapidly in the control group, but not in the *miR-148a*/copGFP group, suggesting that *miR-148a* overexpression impairs tumor relapse after chemotherapy. Analysis of GFP-positive tumor cells collected at day 33 showed that, although the proportion of ALDH-positive cells was significantly increased in FIRI-treated compared with vehicle-treated CTRL/copGFP tumors, this enrichment was impaired in tumors derived from the *miR-148a*/copGFP group (Figure 4D). We also tested the self-renewal ability

and tumorigenic potential of cells collected from FIRI-treated tumors using sphere formation assays *in vitro* and re-transplantation into second generation mice *in vivo*. We first observed that sphere formation was strongly decreased in cells collected from the FIRI-treated *miR-148a*/copGFP tumors (Figure 4E). In agreement, when challenged *in vivo* for tumor initiation in subcutaneous xenograft assays (200 or 2,000 cells/mouse, n = 5 per condition), we observed (Table S1) that the frequency of CSCs in the residual FIRI-treated tumors was ~5 times lower in miR-148a-derived tumors cells than in CTRL tumor cells ($p = 0.006$). These results clearly indicate that *miR-148a* overexpression may represent an efficient strategy to decrease CSC chemoresistance and prevent post-treatment recurrence.

High-content screening identifies niclosamide as a pharmacological inducer of endogenous miR-148a expression

One of the major challenges of synthetic miRNA-based therapy is to achieve efficient systemic delivery in whole organisms. An optional strategy to the direct administration of synthetic miR-148a could reside in the identification of pharmacological *miR-148a* inducers. To identify such compounds, we developed an imaging-based high-content screening assay using a lentiviral *miR-148a-3p* ratio-metric fluorescent sensor. The sensor features a bidirectional promoter to express simultaneously a GFP from *Aequorea coerulescens* (GFP) and the dsRed1 red fluorescent protein (Magill et al., 2010). In the 3′ UTR of the GFP transcript, we incorporated two *miR-148a-3p* recognition elements that correspond to the mature miR-148a sequence (Figure 5A). Thus, the level of GFP reflects the activity of the *miR-148a*, while the dsRed1 signal is used to normalize and minimize the effects of variable expression levels and nonspecific transcriptional regulation, providing a ratiometric measure (GFP/dsRed). We generated a CPP1 patient-derived cancer cell line stably expressing the *miR-148a-3P* sensor construct. As shown in Figures 5A and S4A, we observed a significant decrease of GFP/dsRed ratio when cells were transfected with *miR-148a* mimic compared with mirVana microRNA Mimic Negative Control #1 (miCTRL), thus validating our assay. In addition, using fluorescence-activated cell sorting (FACS), we confirmed the preferential expression of *miR-148a-3p* in $dsRed^{+}GFP^{-}$ compared with $dsRed^{+}GFP^{+}$ cells (Figure 5B), and inversely a lower expression of *miR-148a* target gene mRNAs: *DNMT1* and *PXR* (Figure 5C). These data confirm not only that our *miR-148a-3p* ratio-metric fluorescent sensor provides accurate and quantitative in-cell measurement of *miR-148a* expression but also proves directly the inverse correlation between *miR-148a-3p* and *PXR* expression in sorted cells. We next used this functional tool to screen the Prestwick Chemical Library, which contains 1,280 molecules with known bioavailability and safety in humans. Cells were plated in 384 wells and then treated with 5 μM of each compound for 48 h, followed by fixation, DAPI labeling of nuclei, and image acquisitions and analysis with a high-content screen automated microscope. We identified 10 compounds that significantly reduced the GFP/dsRed ratio (Z score < -2 and $p < 0.05$; Figure 5D; Table S2). We then performed RT-qPCR to measure their effects on endogenous *miR-148a* expression and *miR-148a* target gene expression. As shown in Figure S4B, only niclosamide significantly increased *miR-148a* expression in CPP1 cells compared with vehicle treatment. Accordingly, we observed a decrease in both *DNMT1* and *PXR* mRNA expression in niclosamide-treated cells (Figure S4C). Indeed, niclosamide-mediated *miR-148a* induction (Figure 5E) and *PXR* mRNA inhibition (Figures S4D and S4E) were confirmed on several CRC cells. In agreement, we observed a significant decrease of PXR protein level after 5 μM niclosamide treatment (Figure 5F).

Amazingly, this drug was already pulled out of the Prestwick Library as a potential CRC metastasis blocker (Sack et al., 2011), as well as a potential inhibitor of both *WNT/β-CATENIN* (Osada et al., 2011) and *NOTCH* (Wang et al., 2009) pathways. To verify the direct involvement of *miR-148a* on niclosamide-mediated down-regulation of PXR, we used antagomir-148a, i.e., a chemically modified single-stranded RNA molecule designed to specifically bind to and inhibit endogenous *miR-148a-3p* molecule (anti-miR miRNA inhibitor). Cells were first transfected with the antagomir to block specifically *miR-148a-3p* activity (anti-miR-148a) or a negative control (anti-miR miRNA Inhibitor Negative Control #1 [anti-miCTRL]) prior to niclosamide treatment. As shown in Figures 5G, S4E, and S4F, while niclosamide significantly down-regulated *PXR* mRNA and protein levels in cells transfected with the control sequence (anti-miCTRL), it has a negligible effect in cells transfected with the miR-148a inhibitor. These results demonstrate that the upregulation of miR-148a is crucial for niclosamide-mediated inhibition of PXR expression. In contrast, the *miR-148a* antagomir was unable to antagonize the inhibitory effect of niclosamide on both WNT (*LGR5*, *CCND1*, *JAG1*) and NOTCH (*HES1*, *SURVIVIN*) target gene expression (Figure 5G), suggesting a *miR-148a*-independent pathway(s) in those effects. Overall, these results demonstrate that, although further studies are needed to decipher how niclosamide induces *miR-148a*, its inhibitory effect on PXR expression directly involves *miR-148a* expression.

Niclosamide inhibits PXR activity and the CSC phenotype

Having established the induction of *miR-148a* and the inhibition of PXR expression by niclosamide in CRC cells,

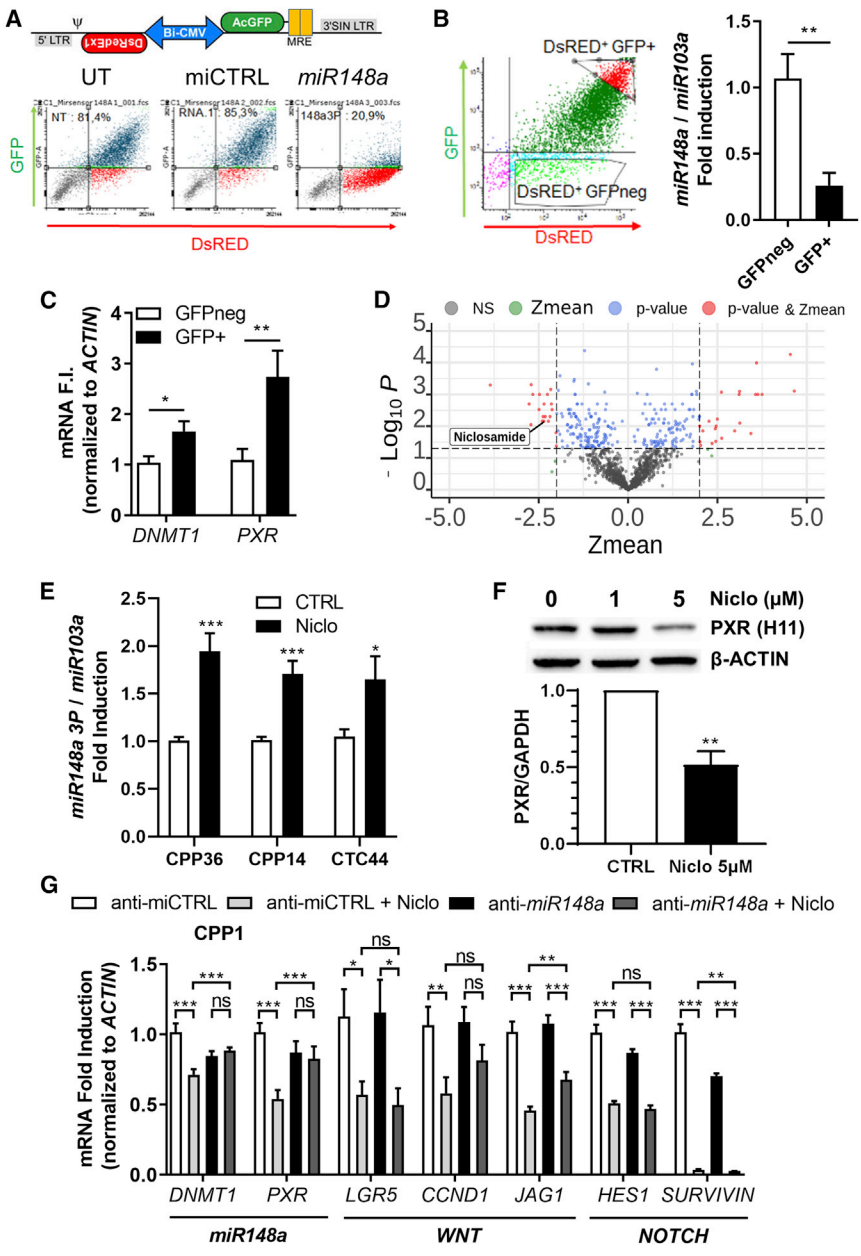

Figure 5. A microscopy-based high-content screen of the Prestwick Chemical Library identifies niclosamide as a pharmacological inducer of endogenous miR-148a

(A–C) Schematic representation of the *miR-148a-3P* mirsensor reporter construct (upper panel). Flow cytometry profiles (GFP versus dsRed) of CPP1 cells stably expressing the *miR-148a-3P* sensor construct transfected with miR-148a or mirVana microRNA Mimic Negative Control #1 (miCTRL) mimics (lower panel) (A). dsRed^{+}GFP^{neg} and dsRed^{+}GFP^{+} cells were double sorted as shown in the chart and then subjected to RT-qPCR analyses of *miR-148a-3P* (B) or *DNMT1* and *PXR* (C). Data are expressed as mean ± SEM (n = 3).

(D) Volcano plot of the retrieved high-content screening data, plotting the negative $\log_{10}$ of the p value against *Z* score (mean of four replicates) on GFP/dsRed signal ratios in response to Prestwick chemical compounds treatment (10 μM, 48 h of treatment). The red dots represent chemical compounds that significantly negatively or positively affect the *Z* score > 2-fold.

(E) RT-qPCR analyses of *miR-148a-3P* expression in patient-derived CPP14 and CPP36 colon cancer cells or circulating tumor cell line (CTC44) treated for 72 h with vehicle (0.1% DMSO = CTRL) or 5 μM niclosamide (Niclo). Data are expressed as mean ± SEM (n = 3).

(F) Western blot analysis of PXR and β-ACTIN expression (upper panel) and relative PXR/β-ACTIN protein ratio (lower panel) in LS174T cells treated for 72 h with vehicle (0.1% DMSO = CTRL) or niclosamide (Niclo) at the indicated final concentrations (mean ± SEM, n = 3).

(G) RT-qPCR analyses on mRNAs expression in CPP1 cells transfected with anti-*miR-148a* or anti-miCTRL and treated 24 h after transfection with vehicle (CTRL = 0.1% DMSO) or 5 μM niclosamide (Niclo) over 48 h. Data are expressed as mean ± SEM (n = 3). *p < 0.05, **p < 0.005, ***p < 0.001.

we then tested its impact on the colon CSC phenotype. As shown in Figures 6A and 6B, niclosamide decreased *PXR* and *DNMT1* mRNA expression in LS174T and CPP1 cells in a dose-dependent manner. Accordingly, the expressions of *ALDH1A1* mRNA and ALDH-positive cells were also reduced after niclosamide treatment in CPP1 (Figure 6C) or CPP14, CPP36, and CTC44 cells (Figures S5A and S5B). In addition, as shown in Figure S5C, the inhibitory effect of niclosamide onto the ALDH-positive cells requires miR-148a induction because this inhibitory effect was abolished in a cell line stably transfected with a *PXR* cDNA construct devoid of the 3′UTR miR-148a-targeting sequence (LS174T-PXR) (Planque et al., 2016). Finally, as observed with the miR-148a mimic, niclosamide treatment significantly reduced the *CD44v6* mRNA and CD44v6-positive populations (Figures 6D and S5D), as well as sphere-forming CRC cells (Figures 6E and 6F). As shown, niclosamide significantly decreased sphere

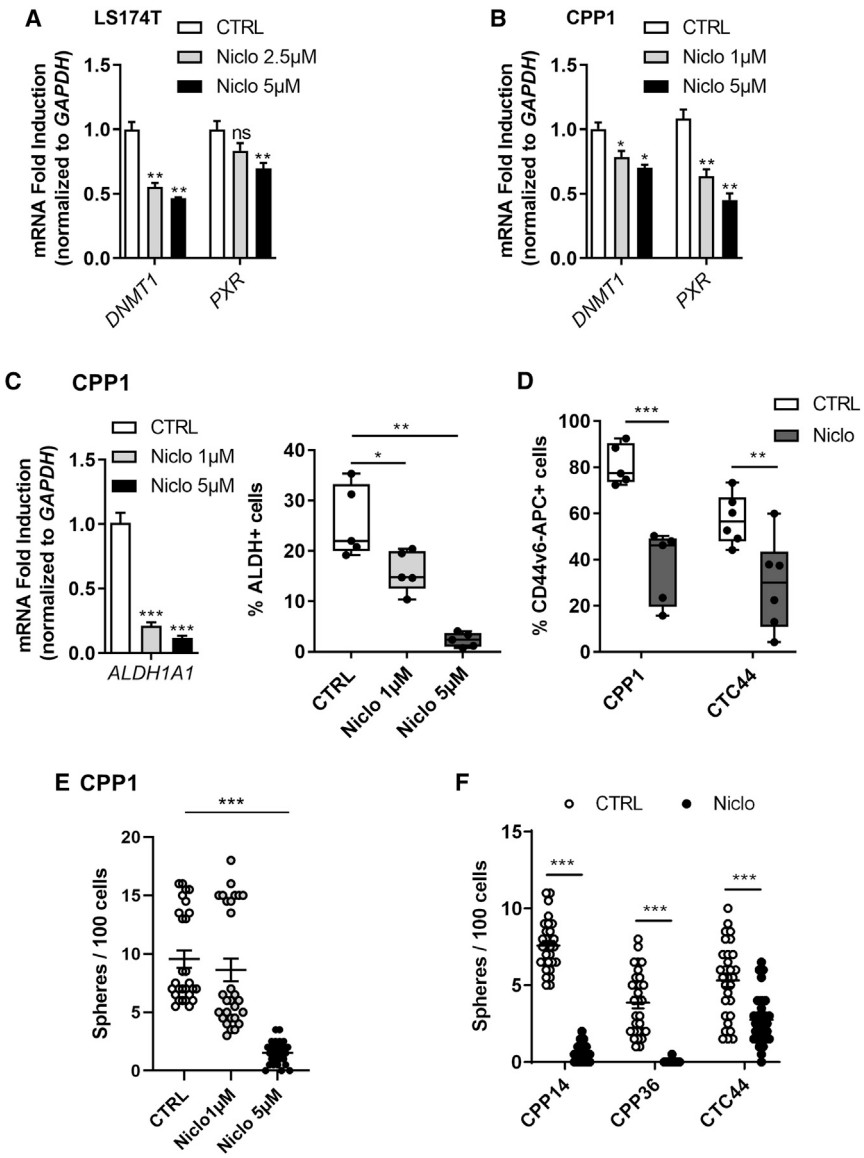

Figure 6. Niclosamide (Niclo) inhibits PXR expression and colon cancer stemness

(A–C) *DNMT1* and *PXR* mRNA expression in LS174T (A) and CPP1 colon cancer cells (B) treated for 72 h with vehicle (0.1% DMSO = CTRL) or Niclo at the indicated final concentrations. Data are expressed as mean ± SEM of three independent experiments. (C, left panel) *ALDH1A1* mRNA expression (n = 3) and (right panel) percentage of Aldefluor-positive cells (% of ALDH + cells, n = 5) in CPP1 colon cancer cells treated for 72 h with vehicle (0.1% DMSO = CTRL) or Niclo at the indicated final concentrations. Data are expressed as mean ± SEM.

(D) Quantification of CD44v6-APC-positive cells in CPP1 or CTC44 cells treated for 72 h with vehicle (0.1% DMSO = CTRL) or 5 μM Niclo. Data are expressed as mean ± SEM (n = 5 for CPP1, n = 6 for CTC44).

(E) Percentage of sphere-forming cells of sorted live (Sytox Blue negative) CPP1 cells, pretreated for 72 h with vehicle (0.1% DMSO = CTRL) or Niclo at the indicated final concentrations. Data are expressed as mean ± SEM, n = 3 (10 individual replicate values per experiment).

(F) Percentage of sphere-forming cells of sorted live (Sytox Blue negative) patient-derived cells (CPP14, CPP36, or CTC44), pretreated for 72 h with vehicle (0.1% DMSO = CTRL) or 5 μM Niclo. Data are expressed as mean ± SEM, n = 3 (10 individual replicate values per experiment). *p < 0.05, **p < 0.005, ***p < 0.001.

formation in a dose-dependent manner, with almost a complete suppression at the highest dose (5 μM) in all CRC cell lines tested.

Niclosamide prevents chemotherapy-induced enrichment of CSCs and delays post-treatment recurrence in mouse xenograft models

We tested the impact of niclosamide on CSC chemoresistance and post-treatment relapse in our preclinical mouse xenograft models. We subcutaneously xenografted 15,000 CPP1 cells from spheroids and allowed tumor volume to reach 100 mm^3 (day 0). Mice were then exposed to the following treatment regimens: PBS (n = 5 mice, CTRL), FIRI alone (n = 10 mice, 50 mg/kg 5-FU and 25 mg/kg irinotecan, twice a week, i.e., Tuesdays and Fridays), niclosamide alone (n = 5 mice, NICLO: 20 mg/kg, 5 days/week, i.e., Mondays to Fridays), or combined niclosamide + FIRI (n = 10 mice, NICLO + FIRI) (Figure 7A). First, we observed that tumor growth was slightly slower in the NICLO group than in the CTRL group. Importantly, we did not observe any clinical signs of toxicity during these 4 weeks of treatment (body weight, diarrhea, skin ulcers, hyper/hypoactivity, changes in motor activity). Six hours after the last treatment (day 29), six FIRI-treated mice per group (+/− niclosamide) were sacrificed for subsequent analyses, while tumor growth and post-treatment relapse were monitored in the remaining mice. Tumor relapse was clearly noticeable from ~2.5 weeks post-treatment (day 46), especially in the group of mice treated with FIRI alone. However, combination of niclosamide treatment with FIRI significantly

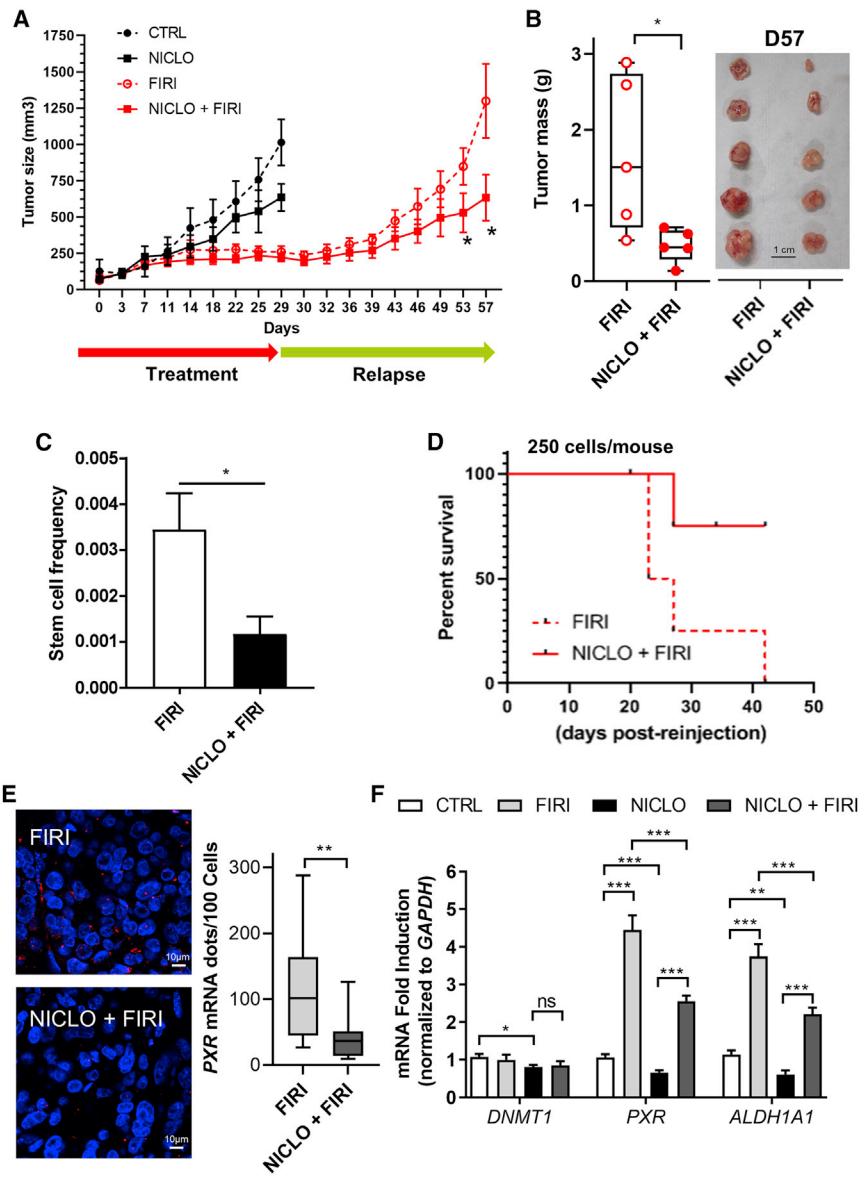

Figure 7. Niclosamide prevents chemotherapy-induced enrichment of CSCs and delays post-treatment recurrence

(A) Tumor volume over time after subcutaneous injection of CPP1 cells. CTRL group (5 mice) was treated four times a week with vehicle (PBS), NICLO group (5 mice) was treated four times a week with niclosamide (20 mg/kg), FIRI group (10 mice) was treated twice a week with chemotherapy (50 mg/kg 5-FU and 25 mg/kg irinotecan), and NICLO + FIRI group (10 mice) was co-treated with niclosamide (20 mg/kg, 4 times a week) plus chemotherapy (50 mg/kg 5-FU and 25 mg/kg irinotecan, twice a week). Tumor volume is expressed as mean ± SEM.

(B) Tumor mass (left panel) and pictures of tumor samples collected at day 57 (right panel) (A).

(C) Cancer stem cell frequency determined by extreme dilution sphere formation assay *in vitro*, performed with pooled live (7AAD-negative) tumor cells isolated from chemotherapy-treated mice at day 29 (FIRI versus NICLO + FIRI). Data are expressed as mean ± SEM, n = 3 (10 replicate values/cell density).

(D) Kaplan-Meier "survival plot" (percentage of mice with no detectable xenograft tumor) after secondary injection of 250 live (7AAD-negative) cells isolated from chemotherapy-treated tumors at day 29, processed for cell dissociation, pooled, and subcutaneously re-implanted in immunodeficient mice (5 mice/group).

(E) Left panel: *PXR* mRNAs (red dots) were detected in CPP1 xenograft tumors collected at day 29 (A) using RNAscope probes and signal amplification system. Nuclei were counterstained with DAPI (blue). Original magnification, ×40. Quantification of *PXR* mRNA signals/100 cells is indicated in the right panel (mean ± SEM, four slides/conditions).

(F) *DNMT1*, *PXR*, and *ALDH1A1* mRNA expression were quantified by RT-qPCR on cells isolated from dissociated xenograft tumors at day 29 (A). Data are expressed as mean ± SEM (n = 5). *p < 0.05, **p < 0.005, ***p < 0.001.

delayed tumor relapse compared with mice treated with chemotherapy alone, leading to a significant reduction of tumor volume and weight at day 57 (Figure 7B). We then analyzed the reservoir of CSCs from tumors collected after the chemotherapy (day 29). After tumor dissociation, live tumor cells (7AAD [(7-aminoactinomycin D]-negative) were purified using a cell sorter, pooled, and then challenged *in vitro* for their ability to form spheres and *in vivo* for tumor initiation in a secondary xenograft assay. As shown in Figure 7C, sphere formation was strongly reduced in cells isolated from the NICLO + FIRI-treated tumors with a 3-fold reduction of CSC frequency quantified using ELDA (Hu and Smyth, 2009) compared with cells isolated from FIRI-treated tumors. In agreement, secondary injection of 250 cells/mouse (Figure 7D) isolated from the niclosamide + FIRI-treated tumors produced fewer tumors than cells recovered from FIRI-treated mice, demonstrating that niclosamide co-treatment decreased the proportion of tumorigenic cells after chemotherapy treatment. Indeed, both RNAscope (Figure 7E) and RT-qPCR (Figure 7F) analyses confirmed that *PXR* mRNA expression was significantly reduced in tumors resected from mice co-treated

with niclosamide and FIRI compared with FIRI-treated tumors. Moreover, we observed that the increase in *PXR* and *ALDH1A1* mRNA expression after FIRI treatment was severely hampered when mice were pretreated with niclosamide, suggesting that niclosamide-mediated PXR down-regulation decreases the preferential survival of CSCs during chemotherapy. These results were confirmed *in vitro* on several patient-derived cells (CPP1, CPP14, CPP36, and CTC44). Although the proportion of ALDH-positive cells was significantly increased after chemotherapy (Firi = 5-FU + SN38) treatment, this enrichment was abolished when cells were pretreated with 5 μM niclosamide (Figure S6A). In agreement, RT-qPCR revealed that the increase in *PXR* and *ALDH1A1* mRNA expression after Firi treatment was also severely hampered when cells were pretreated with niclosamide (Figure S6B). Taken together, these results indicate that repurposing niclosamide as an adjuvant therapy combined with chemotherapy decreases the pool of chemoresistant CSCs, delaying tumor relapse.

DISCUSSION

Although considerable progress has been made in its diagnosis and treatment, metastatic CRC remains characterized by high incidence, low sensitivity to therapy, high risk of developing resistance to chemotherapy, treatment failure, and a low 5-year survival rate (Siegel et al., 2017), making CRC a medical challenge and necessitating the discovery or development of effective treatment strategies. Accumulating studies demonstrated that CSCs, a cancer cell subpopulation with unlimited capacity for self-renewal, differentiation, and tumorigenesis, is one of the reasons for relapse and metastasis (Adorno-Cruz et al., 2015; Dylla et al., 2008; Planque et al., 2016; Prud'homme, 2012; Todaro et al., 2007). In a previous study, we demonstrated that relapse-prone CSCs are characterized by high PXR expression and activity, and this nuclear receptor drives the expression of a large network of genes that are instrumental for CSC chemoresistance (Planque et al., 2016). Thus, decreasing PXR expression/activity using pharmacological inhibitors may represent a promising strategy to improve the efficiency of conventional chemotherapy in CRC patients through the sensitization of CSCs. To inhibit the action of PXR, we developed here an alternative and innovative strategy to those focusing on small-molecule antagonists based on the epigenetic modulation of *PXR* by a miRNA.

We are the first to demonstrate that *miR-148a-3p* expression is down-regulated in colon CSCs (Figure 1) and confirmed that its upregulation regulates negatively PXR expression and activity (Figure 2). In addition, we observed that *miR-148a* significantly affects colon CSC phenotype (Figure 3) by reducing Aldefluor activity, CD44v6 expression, and self-renewal. These results confirm the observation previously reported on a colon cancer cell line (SW480) showing that miR-148a suppresses the expression of stem cell markers and increases their chemo-sensitivity (Shi et al., 2019). These observations agree with previous reports showing the inhibitory effect of *miR-148a* on key CSC signaling pathways, such as WNT/β-CATENIN (Peng et al., 2017) or STAT3 (He and Xue, 2017). Furthermore, we observed that overexpression of *miR-148a-3p* decreased CSCs chemoresistance and significantly delayed tumor relapse after chemotherapy treatment in mouse xenograft models (Figure 4). In accordance with our *in vivo* data, it has also been shown that *miR-148a* overexpression inhibited the growth of ovarian OVCAR3 xenograft tumors in nude mice (Zhu et al., 2019).

In vivo delivery of miRNA has unsolved technical issues and so far, they are inappropriate for therapeutic use due to their poor pharmacokinetic properties *in vivo* (Pecot et al., 2011). Therefore, one possible alternative could be the identification of small molecules acting as endogenous miR-148a inducer or activator. To identify such compounds, we developed a microscopy-based high-content screening assay based on a lentiviral dual-green/red fluorescence *miR-148a-3p* sensor strategy. The screening of 1,280 molecules already approved by US Food and Drug Administration (FDA; Chemical Prestwick Library) allowed us to identify niclosamide as a putative miR-148a activator. The advantage of focusing on such drugs is that their safety profile is well understood and clinically manageable, meaning that they could proceed to clinical trials reasonably quickly. For instance, niclosamide is an oral chlorinated salicylanilide anthelmintic agent that inhibits mitochondrial oxidative phosphorylation in the cells of parasitic worms that has been used for decades for the treatment of tapeworms (Li et al., 2014).

As a consequence of endogenous *miR-148a* upregulation, we observed that niclosamide treatment decreases the expression of miR-148a target genes, such as *DNMT1* and *PXR*, in a *miR-148a*-dependent manner (Figures 5 and 6). In addition, niclosamide treatment inhibited CSC features by reducing the expression of key CSC markers, such as Aldefluor activity or CD44v6 and the sphere-forming ability of patient-derived CRC cell lines and circulating tumor cells (Figure 6). These observations confirm previous studies reporting that niclosamide attenuates the tumor-initiating and survival potential of colon CSCs (Arend et al., 2016). Moreover, niclosamide has been reported to decrease the Aldefluor-positive population in breast (Londoño-Joshi et al., 2014) and melanoma (Zhou et al., 2017) cancer cells, and reduced the frequency of both $CD44^{high}/CD24^{low}$ CSC cell population and mammosphere formation in breast cancer cell lines (Liu et al., 2016). Finally, we report that niclosamide co-treatment potentialized frontline

chemotherapeutic agents' efficiency in targeting colon CSCs (Figure 7). Notably, we demonstrated using *in vitro* and *in vivo* (mice xenografts) experiments that niclosamide exhibits remarkable synergism with CRC mainstream anticancer drugs because it sensitizes colon CSCs to chemotherapy drugs, decreasing chemoresistance-related gene expression, and delays tumor relapse after treatment cessation. Our preclinical data strongly suggest that niclosamide could be repurposed as neoadjuvant strategy to potentiate chemotherapeutic drugs for treating CRC, through *miR-148a* induction and the subsequent inhibition of its target genes involved in CSC self-renewal and chemoresistance.

These preclinical data warrant further validation and translation toward clinical trials to confirm their effectiveness in patients. Notably, niclosamide is orally administered to helminthiasis patients, while in our study we used intraperitoneal administration. However, this route of administration has been already successfully used by others, leading to a significant inhibition of tumor growth in human ovarian (Shangguan et al., 2020) and breast cancers transplanted tumor models (Liu et al., 2016). Osada et al. (2011) found that oral administration of niclosamide (200 mg/kg body weight) resulted in sufficient distribution of the drug into murine xenografts. In patients, the serum concentrations of niclosamide are 0.25–6.0 μg/mL (Andrews et al., 1982), corresponding to 0.76–18.35 μM. These concentrations correspond well to the active concentration range for *miR-148a* induction observed in our study (5 μM). Importantly, a phase I clinical trial is currently ongoing to evaluate the maximum tolerated dose of niclosamide in CRC patients (ClinicalTrials.gov: NCT02687009) and a phase II trial (NIKOLO) to investigate the safety and efficacy of orally applied niclosamide in metastatic CRC patients with progressive disease after chemotherapy (Burock et al., 2018). Thus, based on these ongoing studies and on our preclinical work, we believe that additional trials could be designed to investigate clinical opportunities offered by niclosamide repurposing as adjuvant strategy, as *miR-148a* inducer to decrease PXR expression and CSC chemoresistance during chemotherapy in metastatic CRC patients.

EXPERIMENTAL PROCEDURES

See supplemental information for more details.

Staining for flow cytometry analysis and FACS

CD44-allophycocyanin (APC) (559,942; BD Pharmingen), CD44 v6-APC (clone REA706, 130-111-238; Macs Miltenyi), or CD44 v6-phycoerythrin (PE) (FAB3660P; R&D) antibodies (1/100) were incubated with 100,000 cells in PBS containing 5% FBS for 20 min at 4°C. The Aldefluor assay (Stem Cell Technologies) or ALDHRed assay (Millipore) was performed according to the manufacturer's instructions. ALDH-positive and ALDH-negative cells were identified by comparing the same sample with and without the ALDH inhibitor diethylaminobenzaldehyde (DEAB).

Stainings were analyzed using the MACSQUANT (Miltenyi) analyzer. Cells were sorted using a FACSAria II (BD) and analyzed using Flowing software (v 2.5.1; http://flowingsoftware.btk.fi/).

High-content screening

We performed an automated screening of all 1,280 FDA-approved drugs in the Prestwick Chemical Library at 5 μM in black clear-bottom 384-well plates using the CPP1-miR-148a sensor cellular model. This screening was performed with four replicates of each compound, for a total of sixteen 384-well plates using a Tecan EVO200 robotic liquid handling system (Tecan Trading AG). Image analysis and quantifications of output parameters were obtained with High Content Screen Studio Cell Analysis software (v3.0; Thermo Scientific). Image analysis allowed first detecting and counting cells in wells with DAPI nuclear labeling. Then we quantified a cell-by-cell GFP/dsRed1 signal ratio into enlarged nuclear region (region of interest [ROI] + 2 pixels), the specific readout for our screening. "Hits" were identified using the robust *Z* score statistical method on GFP/dsRed1 signal ratio (cf. screening data normalization section in supplemental information).

Xenograft transplantation and combination of niclosamide and chemotherapy treatment

All experiments were performed according to the European Union (Council directive 86/609EEC) and institutional/local guidelines on laboratory animal usage. Animal protocols were approved by the French ethical committee for animal testing (authorization referral #1627). All efforts were directed at minimizing animal discomfort and to reduce the number of animals used (3R rule). Cells in suspension were injected subcutaneously into the right flanks on NOD/SCID mice (Charles River) in a 1:1 mixture of Matrigel and DMEM in a final volume of 100 μL. Tumor volume ([length × width^2]/2) was measured with a caliper. Randomization and treatment started once tumor volume reached 100 mm^3, and mice were sacrificed when tumors reached 1,500 mm^3.

Statistical analysis

For each experiment, data are shown as mean ± SEM of n independent experiments (n = number of independent experiments). GraphPad Prism7 software was used for data analysis. The Mann-Whitney test was used to analyze the difference between two groups of quantitative variables with alpha value set at 5%: *$p < 0.05$, **$p < 0.005$, ***$p < 0.001$.

SUPPLEMENTAL INFORMATION

Supplemental information can be found online at https://doi.org/10.1016/j.stemcr.2022.02.005.

AUTHOR CONTRIBUTIONS

C.P., J.M.P., and J.P. designed the research; C.P., J.M.P., and J.P. designed part of the experiments; L.B., O.B., E.M., G.L.G., A.G., E.P., M.B., B.B., J.M.P., and C.P. performed the experiments; L.B., O.B., E.M., G.L.G., A.G., E.P., M.B., C.H.-K., B.B., J.P., J.M.P., and C.P.

analyzed the data; J.F.B. and M.P. provided reagents/analytic tools; F.H., J.P., J.M.P., and C.P. wrote the manuscript.

CONFLICTS OF INTERESTS

The authors declare no competing interests.

ACKNOWLEDGMENTS

We acknowledge the contribution of iExplore animal facility (IGF, Montpellier) and the AniRA lentivectors production facility from the CELPHEDIA Infrastructure and SFR Biosciences (UMS3444/CNRS, US8/INSERM, ENS de Lyon, UCBL). We thank C. Duperray (IRBM, Montpellier) from the Montpellier RIO Imaging platform for flow cytometry experiments and Jérôme Torrisani (INSERM UMR 1037, University of Toulouse III, France) for the gift of MIR148a-copGFP and pMIRNA1-copGFP. This work was supported by grants from the INCa, Cancéropôle GSO, Association pour la Recherche contre le Cancer, Key Initiative Muse "Biomarkers and Therapy," GEFLUC, and SIRIC of Montpellier (France).

Received: March 30, 2021
Revised: February 4, 2022
Accepted: February 7, 2022
Published: March 10, 2022

REFERENCES

Adorno-Cruz, V., Kibria, G., Liu, X., Doherty, M., Junk, D.J., Guan, D., Hubert, C., Venere, M., Mulkearns-Hubert, E., Sinyuk, M., et al. (2015). Cancer stem cells: targeting the roots of cancer, seeds of metastasis, and sources of therapy resistance. Cancer Res. *75*, 924–929.

Andrews, P., Thyssen, J., and Lorke, D. (1982). The biology and toxicology of molluscicides, Bayluscide. Pharmacol. Ther. *19*, 245–295.

Arend, R.C., Londoño-Joshi, A.I., Gangrade, A., Katre, A.A., Kurpad, C., Li, Y., Samant, R.S., Li, P.K., Landen, C.N., Yang, E.S., et al. (2016). Niclosamide and its analogs are potent inhibitors of Wnt/β-catenin, mTOR and STAT3 signaling in ovarian cancer. Oncotarget *7*, 86803–86815.

Boo, L., Ho, W.Y., Mohd Ali, N., Yeap, S.K., Ky, H., Chan, K.G., Yin, W.F., Satharasinghe, D.A., Liew, W.C., Tan, S.W., et al. (2017). Phenotypic and microRNA transcriptomic profiling of the MDA-MB-231 spheroid-enriched CSCs with comparison of MCF-7 microRNA profiling dataset. PeerJ *5*, e3551.

Burock, S., Daum, S., Keilholz, U., Neumann, K., Walther, W., and Stein, U. (2018). Phase II trial to investigate the safety and efficacy of orally applied niclosamide in patients with metachronous or sychronous metastases of a colorectal cancer progressing after therapy: the NIKOLO trial. BMC Cancer *18*, 297.

Dong, Y., Wang, Z., Xie, G.F., Li, C., Zuo, W.W., Meng, G., Xu, C.P., and Li, J.J. (2017). Pregnane X receptor is associated with unfavorable survival and induces chemotherapeutic resistance by transcriptional activating multidrug resistance-related protein 3 in colorectal cancer. Mol. Cancer *16*, 71.

Drocourt, L., Ourlin, J.C., Pascussi, J.M., Maurel, P., and Vilarem, M.J. (2002). Expression of *CYP3A4*, CYP2B6, and CYP2C9 is regulated by the vitamin D receptor pathway in primary human hepatocytes. J. Biol. Chem. *277*, 25125–25132.

Dylla, S.J., Beviglia, L., Park, I.K., Chartier, C., Raval, J., Ngan, L., Pickell, K., Aguilar, J., Lazetic, S., Smith-Berdan, S., et al. (2008). Colorectal cancer stem cells are enriched in xenogeneic tumors following chemotherapy. PLoS One *3*, e2428.

Fuchs, I., Hafner-Blumenstiel, V., Markert, C., Burhenne, J., Weiss, J., Haefeli, W.E., and Mikus, G. (2013). Effect of the CYP3A inhibitor ketoconazole on the *PXR*-mediated induction of CYP3A activity. Eur. J. Clin. Pharmacol. *69*, 507–513.

Ginestier, C., Hur, M.H., Charafe-Jauffret, E., Monville, F., Dutcher, J., Brown, M., Jacquemier, J., Viens, P., Kleer, C.G., Liu, S., et al. (2007). ALDH1 is a marker of normal and malignant human mammary stem cells and a predictor of poor clinical outcome. Cell Stem Cell *1*, 555–567.

Grillet, F., Bayet, E., Villeronce, O., Zappia, L., Lagerqvist, E.L., Lunke, S., Charafe-Jauffret, E., Pham, K., Molck, C., Rolland, N., et al. (2017). Circulating tumour cells from patients with colorectal cancer have cancer stem cell hallmarks in ex vivo culture. Gut *66*, 1802–1810.

He, M., and Xue, Y. (2017). MicroRNA-148a suppresses proliferation and invasion potential of non-small cell lung carcinomas via regulation of STAT3. Onco Targets Ther. *10*, 1353–1361.

Hu, Y., and Smyth, G.K. (2009). ELDA: extreme limiting dilution analysis for comparing depleted and enriched populations in stem cell and other assays. J. Immunol. Methods *347*, 70–78.

Huang, W. (2017). MicroRNAs: biomarkers, diagnostics, and therapeutics. Methods Mol. Biol. (Clifton, NJ) *1617*, 57–67.

Huang, H., Wang, H., Sinz, M., Zoeckler, M., Staudinger, J., Redinbo, M.R., Teotico, D.G., Locker, J., Kalpana, G.V., and Mani, S. (2007). Inhibition of drug metabolism by blocking the activation of nuclear receptors by ketoconazole. Oncogene *26*, 258–268.

Igder, S., Mohammadiasl, J., and Mokarram, P. (2019). Altered miR-21, miRNA-148a expression in relation to KRAS mutation status as indicator of adenoma-carcinoma transitional pattern in colorectal adenoma and carcinoma lesions. Biochem. Genet. *57*, 767–780.

Kanwar, S.S., Yu, Y., Nautiyal, J., Patel, B.B., and Majumdar, A.P. (2010). The Wnt/beta-catenin pathway regulates growth and maintenance of colonospheres. Mol. Cancer *9*, 212.

Kreso, A., O'Brien, C.A., van Galen, P., Gan, O.I., Notta, F., Brown, A.M., Ng, K., Ma, J., Wienholds, E., Dunant, C., et al. (2013). Variable clonal repopulation dynamics influence chemotherapy response in colorectal cancer. Science *339*, 543–548.

Lehmann, J.M., McKee, D.D., Watson, M.A., Willson, T.M., Moore, J.T., and Kliewer, S.A. (1998). The human orphan nuclear receptor *PXR* is activated by compounds that regulate *CYP3A4* gene expression and cause drug interactions. J. Clin. Invest. *102*, 1016–1023.

Li, Y., Li, P.K., Roberts, M.J., Arend, R.C., Samant, R.S., and Buchsbaum, D.J. (2014). Multi-targeted therapy of cancer by niclosamide: a new application for an old drug. Cancer Lett. *349*, 8–14.

Lin, W., Wang, Y.M., Chai, S.C., Lv, L., Zheng, J., Wu, J., Zhang, Q., Wang, Y.D., Griffin, P.R., and Chen, T. (2017). SPA70 is a potent antagonist of human pregnane X receptor. Nat. Commun. *8*, 741.

Liu, J., Chen, X., Ward, T., Mao, Y., Bockhorn, J., Liu, X., Wang, G., Pegram, M., and Shen, K. (2016). Niclosamide inhibits epithelial-mesenchymal transition and tumor growth in lapatinib-resistant human epidermal growth factor receptor 2-positive breast cancer. Int. J. Biochem. Cell Biol. *71*, 12–23.

Londoño-Joshi, A.I., Arend, R.C., Aristizabal, L., Lu, W., Samant, R.S., Metge, B.J., Hidalgo, B., Grizzle, W.E., Conner, M., Forero-Torres, A., et al. (2014). Effect of niclosamide on basal-like breast cancers. Mol. Cancer Ther. *13*, 800–811.

Ma, L., Dong, L., and Chang, P. (2019). CD44v6 engages in colorectal cancer progression. Cell Death Dis. *10*, 30.

Magill, S.T., Cambronne, X.A., Luikart, B.W., Lioy, D.T., Leighton, B.H., Westbrook, G.L., Mandel, G., and Goodman, R.H. (2010). microRNA-132 regulates dendritic growth and arborization of newborn neurons in the adult hippocampus. Proc. Natl. Acad. Sci. U S A *107*, 20382–20387.

Osada, T., Chen, M., Yang, X.Y., Spasojevic, I., Vandeusen, J.B., Hsu, D., Clary, B.M., Clay, T.M., Chen, W., Morse, M.A., et al. (2011). Antihelminth compound niclosamide downregulates Wnt signaling and elicits antitumor responses in tumors with activating APC mutations. Cancer Res. *71*, 4172–4182.

Pecot, C.V., Calin, G.A., Coleman, R.L., Lopez-Berestein, G., and Sood, A.K. (2011). RNA interference in the clinic: challenges and future directions. Nat. Rev. Cancer *11*, 59–67.

Peng, L., Liu, Z., Xiao, J., Tu, Y., Wan, Z., Xiong, H., Li, Y., and Xiao, W. (2017). MicroRNA-148a suppresses epithelial-mesenchymal transition and invasion of pancreatic cancer cells by targeting Wnt10b and inhibiting the Wnt/β-catenin signaling pathway. Oncol. Rep. *38*, 301–308.

Planque, C., Rajabi, F., Grillet, F., Finetti, P., Bertucci, F., Gironella, M., Lozano, J.J., Beucher, B., Giraud, J., Garambois, V., et al. (2016). Pregnane X-receptor promotes stem cell-mediated colon cancer relapse. Oncotarget *7*, 56558–56573.

Poulton, E.J., Levy, L., Lampe, J.W., Shen, D.D., Tracy, J., Shuhart, M.C., Thummel, K.E., and Eaton, D.L. (2013). Sulforaphane is not an effective antagonist of the human pregnane X-receptor in vivo. Toxicol. Appl. Pharmacol. *266*, 122–131.

Prud'homme, G.J. (2012). Cancer stem cells and novel targets for antitumor strategies. Curr. Pharm. Des. *18*, 2838–2849.

Rao, Z.Z., Zhang, X.W., and Ding, Y.L. (2017). miR-148a-mediated estrogen-induced cholestasis in intrahepatic cholestasis of pregnancy: role of *PXR*/MRP3. PLoS One *12*, e0178702.

Reuter, T., Herold-Mende, C., Dyckhoff, G., Rigalli, J.P., and Weiss, J. (2019). Functional role of miR-148a in oropharyngeal cancer: influence on pregnane X receptor and P-glycoprotein expression. J. Recept. Signal Transduct. Res. *39*, 451–459.

Sack, U., Walther, W., Scudiero, D., Selby, M., Kobelt, D., Lemm, M., Fichtner, I., Schlag, P.M., Shoemaker, R.H., and Stein, U. (2011). Novel effect of antihelminthic Niclosamide on S100A4-mediated metastatic progression in colon cancer. J. Natl. Cancer Inst. *103*, 1018–1036.

Shangguan, F., Liu, Y., Ma, L., Qu, G., Lv, Q., An, J., Yang, S., Lu, B., and Cao, Q. (2020). Niclosamide inhibits ovarian carcinoma growth by interrupting cellular bioenergetics. J. Cancer *11*, 3454–3466.

Shi, L., Xi, J., Xu, X., Peng, B., and Zhang, B. (2019). MiR-148a suppressed cell invasion and migration via targeting WNT10b and modulating β-catenin signaling in cisplatin-resistant colorectal cancer cells. Biomed. Pharmacother. *109*, 902–909.

Shivapurkar, N., Weiner, L.M., Marshall, J.L., Madhavan, S., Deslattes Mays, A., Juhl, H., and Wellstein, A. (2014). Recurrence of early stage colon cancer predicted by expression pattern of circulating microRNAs. PLoS One *9*, e84686.

Siegel, R.L., Miller, K.D., Fedewa, S.A., Ahnen, D.J., Meester, R.G.S., Barzi, A., and Jemal, A. (2017). Colorectal cancer statistics, 2017. CA Cancer J. Clin. *67*, 177–193.

Takagi, S., Nakajima, M., Mohri, T., and Yokoi, T. (2008). Post-transcriptional regulation of human pregnane X receptor by microRNA affects the expression of cytochrome P450 3A4. J. Biol. Chem. *283*, 9674–9680.

Takahashi, M., Cuatrecasas, M., Balaguer, F., Hur, K., Toiyama, Y., Castells, A., Boland, C.R., and Goel, A. (2012). The clinical significance of MiR-148a as a predictive biomarker in patients with advanced colorectal cancer. PLoS One *7*, e46684.

Todaro, M., Alea, M.P., Di Stefano, A.B., Cammareri, P., Vermeulen, L., Iovino, F., Tripodo, C., Russo, A., Gulotta, G., Medema, J.P., et al. (2007). Colon cancer stem cells dictate tumor growth and resist cell death by production of interleukin-4. Cell Stem Cell *1*, 389–402.

Todaro, M., Gaggianesi, M., Catalano, V., Benfante, A., Iovino, F., Biffoni, M., Apuzzo, T., Sperduti, I., Volpe, S., Cocorullo, G., et al. (2014). CD44v6 is a marker of constitutive and reprogrammed cancer stem cells driving colon cancer metastasis. Cell Stem Cell *14*, 342–356.

Tsai, H.L., Yang, I.P., Huang, C.W., Ma, C.J., Kuo, C.H., Lu, C.Y., Juo, S.H., and Wang, J.Y. (2013). Clinical significance of microRNA-148a in patients with early relapse of stage II stage and III colorectal cancer after curative resection. Transl. Res. *162*, 258–268.

Wang, A.M., Ku, H.H., Liang, Y.C., Chen, Y.C., Hwu, Y.M., and Yeh, T.S. (2009). The autonomous notch signal pathway is activated by baicalin and baicalein but is suppressed by niclosamide in K562 cells. J. Cell. Biochem. *106*, 682–692.

Wang, H., Venkatesh, M., Li, H., Goetz, R., Mukherjee, S., Biswas, A., Zhu, L., Kaubisch, A., Wang, L., Pullman, J., et al. (2011). Pregnane X receptor activation induces *FGF19*-dependent tumor aggressiveness in humans and mice. J. Clin. Invest. *121*, 3220–3232.

Yan, J., Guo, X., Xia, J., Shan, T., Gu, C., Liang, Z., Zhao, W., and Jin, S. (2014). MiR-148a regulates MEG3 in gastric cancer by targeting DNA methyltransferase 1. Med. Oncol. *31*, 879.

Zhou, C., Poulton, E.J., Grün, F., Bammler, T.K., Blumberg, B., Thummel, K.E., and Eaton, D.L. (2007). The dietary isothiocyanate sulforaphane is an antagonist of the human steroid and xenobiotic nuclear receptor. Mol. Pharmacol. *71*, 220–229.

Zhou, J., Jin, B., Jin, Y., Liu, Y., and Pan, J. (2017). The antihelminthic drug niclosamide effectively inhibits the malignant phenotypes of uveal melanoma in vitro and in vivo. Theranostics *7*, 1447–1462.

Zhu, D., Yuan, D., Guo, R., Zhang, L., Guo, T., Zhao, Y., Wang, J., Chen, X., Qian, H., and Ge, H. (2019). Overexpression of miR-148a inhibits viability and invasion of ovarian cancer OVCAR3 cells by targeting FOXO3. Oncol. Lett. *18*, 402–410.